Thermal Model Performance for the James Webb Space Telescope OTIS Cryo-Vacuum Test

Kan Yang[1], Stuart D. Glazer[2], Shaun R. Thomson[3], and Lee D. Feinberg[4]
NASA Goddard Space Flight Center, Greenbelt MD 20771

William Burt[5], Brian J. Comber[6], and Wes Ousley[7]
Genesis Engineering Solutions Inc., Lanham, MD 20706

Randy Franck[8]
Ball Aerospace, Boulder, CO 80301

The James Webb Space Telescope (JWST), set to launch in mid-2020, is currently undergoing a series of system-level environmental tests to verify its workmanship and end-to-end functionality. As part of this series, the Optical Telescope Element and Integrated Science Instrument Module (OTIS) Cryo-Vacuum (CV) test, the most complex cryogenic test executed to date by NASA, has recently been completed at the Johnson Space Center's Chamber A facility. The OTIS CV test was intended as a comprehensive test of the integrated instrument and telescope systems to fully understand its optical, structural, and thermal performance within its intended flight environment. Due to its complexity, extensive pre-test planning was required to ensure payload safety and compliance with all limits and constraints. A system-level pre-test thermal model was constructed which fully captured the behavior of the payload, ground support equipment, and surrounding test chamber. This thermal model simulated both the transient cooldown to and warmup from a 20 K flight-like environment, as well as predicted the payload performance at cryo-stable conditions. The current work is an assessment of thermal model pre-test prediction performance against actual payload response during the OTIS CV test. Overall, the thermal model performed exceedingly well at predicting schedule and payload response. Looking in depth, this work examines both the benefits and shortcomings of assumptions made pre-test to simplify model execution when compared against test data. It explores in detail the role of temperature-dependent emissivities during transition to cryogenic temperatures, as well as the impact that model geometry simplifications have on tracking of critical hardware limits and constraints. This work concludes with a list of recommendations to improve the accuracy of thermal modeling for future large cryogenic tests. The insight gained from the OTIS CV test thermal modeling will benefit planning and execution for upcoming cryogenic missions.

Nomenclature

AOS = Aft Optical System
ACF = Auto-Collimating Flat
ADIR = Aft Deployable ISIM Radiator
ASPA = Aft optical system Source Plate Assembly
BP = Back Plane

[1] Thermal Engineer, JWST Project, NASA/GSFC, Code 545

[2] Lead Thermal Systems Engineer, JWST ISIM Element, OTIS Thermal Lead Engineer, NASA/GSFC, Code 545

[3] Lead Thermal Systems Engineer, JWST Project, NASA/GSFC, Code 545

[4] Optical Telescope Element Manager, JWST Project, NASA/GSFC, Code 550

[5] Lead Cryogenic Thermal Systems Engineer, 4501 Boston Way, Lanham, MD 20706

[6] Thermal Engineer, 4501 Boston Way, Lanham, MD 20706

[7] Thermal Systems Engineer, 4501 Boston Way, Lanham, MD 20706

[8] Lead Thermal Systems Engineer, 1600 Commerce St, Boulder, CO 80301

BSF = Backplane Support Fixture
CoCOA = Center of Curvature Optical Assembly
CPP = Cryo-Pumping Panels, separate cold panels between the helium and LN_2 shrouds at NASA JSC
CSA = Canadian Space Agency
CTE = Coefficient of thermal expansion
CV = Cryo-Vacuum
ΔT = Change in temperature
DTA = Deployable Tower Assembly
DSERS = Deep Space Environment Radiative Sink
EC = European Consortium
ESA = European Space Agency
FGS = Fine Guidance Sensor
FIR = Fixed ISIM Radiator
FPA = Focal Plane Arrays
FSM = Fine Steering Mirror
GSE = Ground Support Equipment
GSFC = NASA Goddard Space Flight Center
HOSS = Hardpoint and Offload Support Structure
IEC = ISIM Electronics Compartment
IR = Infrared
ISIM = Integrated Science Instrument Module, which contains the Science Instruments (SIs)
JSC = NASA Johnson Space Center
JWST = James Webb Space Telescope
K = Kelvin
L&Cs = Limits and Constraints
L5 = Layer 5 Sunshield simulator
LN₂ = Liquid Nitrogen
LRM = Launch Release Mechanism
MIRI = Mid-Infrared Instrument
MLI = Multi-Layer Insulation
NASA = National Aeronautics and Space Administration
NGAS = Northrop Grumman Aerospace Systems
NIRCam = Near-Infrared Camera instrument
NIRSpec = Near-Infrared Spectrograph instrument
OA = Optical Assembly
OGSE = Optical Ground Support Equipment, a series of pre-OTIS optical pathfinder tests
OTE = Optical Telescope Element
OTIS = Optical Telescope Element plus Integrated Science Instrument Module (OTE + ISIM)
PG = PhotoGrammetry cameras
POM = Instrument Pick-Off Mirror
PM = Primary Mirror(s)
PMSA = Primary Mirror Segment Assembly
PMBSS = Primary Mirror Backplane Support Structure (BSF + BP)
SI = Science Instrument
SINDA = Systems Improved Numerical Differential Analyzer modeling tool
SM = Secondary Mirror
SMA = Secondary Mirror Assembly
SMSS = Secondary Mirror Support Structure
SVTS = Space Vehicle Thermal Simulator
TM = Tertiary Mirror
TPF = Thermal Pathfinder test
W = Watt(s)

International Conference on Environmental Systems

I. Introduction

THE James Webb Space Telescope (JWST) is NASA's next-generation space telescope. As a collaboration between NASA, the European Space Agency (ESA), the European Consortium (EC), the Canadian Space Agency (CSA), and partners in industry and academia, JWST (Figure 1) will provide scientists with unprecedented capabilities in the mid-to-near infrared bands to image the formation of the first stars and galaxies in the universe and to capture exoplanets. After launch in 2020 atop an Ariane 5 launch vehicle from Kourou, French Guiana, JWST will undergo a series of deployments before entering orbit at the Earth-Sun L2 Lagrange point, about 1.5 million km from Earth. A tennis-court-sized, five layer sunshield will protect the optical telescope and instruments from solar radiation, allowing the cold "telescope" portion of the spacecraft to cool to cryogenic temperatures for its science operations.

JWST has been undergoing extensive cryogenic vacuum tests to verify its ability to withstand the harsh space environment. The size of the fully-deployed observatory makes it prohibitive to test in any existing facility. To ensure that the telescope functions as planned and achieves its design cryogenic temperatures in the space environment, optical and cryo-vacuum verification via two separate system-level assemblies is necessary before its final integration. These tests include the spacecraft bus and the sunshield, comprising the spacecraft element (SCE); and the science instruments and optics, which together form OTIS. As these separate system-level tests replace the full observatory-level test, observatory-level verification is achieved with thermal models correlated through system-level testing. However, this requires an increased level of rigor in the system-level testing to ensure that models can accurately predict the behavior seen at the subsystem and system levels, since JWST relies on analysis to confirm that the observatory-level assembly works as intended.

The OTIS cryo-vacuum (CV) test at NASA JSC's Chamber A facility took place from July through October of 2017, and allowed for the system-level verification of both the Optical Telescope Element (OTE) and the Integrated Science Instrument Module (ISIM), essentially merging the telescope and its four instruments into a fully-integrated science package[1,2]. OTIS CV was the culmination of years of subsystem-level OTE and ISIM cryo-vacuum tests: two Optical Ground Support Equipment (OGSE)[3] tests

Figure 1. The James Webb Space Telescope and its major system-level assemblies

and one Thermal Pathfinder (TPF)[4-6] risk-reduction test at NASA's Johnson Space Center (JSC) for OTE; and three successive ISIM cryo-vacuum tests[7] at NASA's Goddard Space Flight Center (GSFC). OTIS allowed for end-to-end optical testing in the appropriate thermal environment for the combined assembly of the optical telescope and instruments, as well as validation of the thermal design and its ability to achieve expected cryogenic balance temperatures. It further served as a verification of workmanship and as a crosscheck of the assembled and integrated models. For this CV test, there were five thermal control objectives:

1. To preserve hardware integrity upon transition to cryogenic thermal balance (cryo-balance) conditions and transition back to ambient temperatures by respecting all imposed limits and constraints;
2. To achieve the simulated on-orbit payload temperature levels and stability for optical, mechanical, and instrument tests;
3. To predict and measure thermal balance test data for model crosscheck, both on ISIM and OTE components;
4. To achieve a workmanship thermal conductance assessment of the flight instrument heat straps which for the first time would be connecting all the payload flight instruments and radiators;
5. To achieve test timeline optimization by executing the OTIS CV cooldown and warmup in a time-efficient manner.

These thermal control objectives ensured that the test could be executed in a safe, efficient manner over its 100-day duration. However, meeting these objectives required significant predictive capability to address all of the imposed
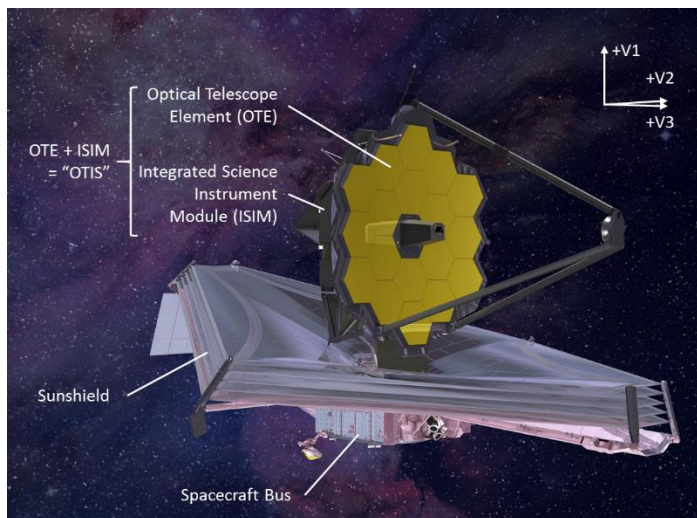
3

Limits and Constraints (L&Cs), including structural gradient, temperature rate-of-change, contamination control, and survival limits. To this end, the OTIS CV thermal model was developed, consisting of an integrated system-level model of the OTIS payload from Northrop Grumman Aerospace Systems (NGAS) with substantial inputs from NASA GSFC, detailed optical component models from Ball Aerospace, and a reduced Ground Support Equipment (GSE) model, including the chamber and facilities, provided by Harris Corporation. The OTIS CV thermal model was generated with Thermal Desktop and SINDA/FLUINT version 5.6, contains over 84,000 nodes, and typically requires more than a week of wall-clock time to run a simulated cooldown profile of 35 days or warmup profile of 20 days. The OTIS CV thermal model predictions were used to develop appropriate cooldown and warmup procedures employing the appropriate thermal control surfaces and methods to transition the OTIS payload from ambient to its cryogenic test conditions and back to ambient[8]. The model was also used to evaluate critical L&Cs: those that lacked flight sensors to monitor real-time during the OTIS CV test were predicted pre-test with sufficient margin to ensure that they could be met during transitions.

The current work will discuss the OTIS CV thermal model's performance against as-measured test data, especially with regards to cooldown and warmup behavior of the payload itself. The system-level model made generally accurate predictions for test duration and hardware performance against L&Cs. However significant simplifications and assumptions needed to be made to ensure timely model predictions and reduce runtime. The lower model complexity and resolution in certain areas also resulted in deviations of model predictions from actual hardware behavior. A discussion of test configuration is provided in the next section to describe the OTIS CV test before examining the most impactful decisions made with regards to thermal modeling.

II. Test Configuration

The OTIS payload encompasses all components of the observatory that lie above the plane of the coldest sunshield layer. Figure 2 shows the OTIS payload in its test configuration at JSC; note the chamber coordinate system in so-called V-coordinates. In the optical path for the telescope element, light reflects off of the 18 gold-coated beryllium Primary Mirror Segments comprising the Primary Mirror Segment Assembly (PMSA), then the Secondary Mirror Assembly (SMA), and lastly enters the Aft Optics Subsystem (AOS), where it travels from the Tertiary Mirror (TM) to the Fine Steering Mirror (FSM) to the pick-off mirrors for each separate science instrument within the ISIM enclosure. The ISIM consists of four instruments mounted to the rigid composite ISIM structure: the Near-Infrared Camera (NIRCam), developed by NASA and the University of Arizona; the Near-Infrared Spectrograph (NIRSpec), a collaboration between the ESA and NASA, separated into its Optical Assembly (OA) and Focal Plane Assembly (FPA) components; the Fine Guidance Sensor (FGS), provided by the Canadian Space Agency; and the Mid-Infrared Instrument (MIRI), jointly sponsored by ESA and the European Consortium.

Structurally, the PMSAs and the AOS are supported by the Backplane (BP), a large thermal insulation-wrapped M55J composite structure comprised of a center section and foldable wings. ISIM is kinematically mounted to the Backplane Support Fixture (BSF), a truss-like composite structure. Together, BP and BSF form the Primary Mirror Backplane Support Structure (PMBSS), the mechanical framework which holds the telescope element and instruments in place. The entire telescope assembly is then interfaced with the flight spacecraft bus and sunshield via the Deployable Tower Assembly (DTA). On the −V1 side of the payload, the room-temperature ISIM Electronics Compartment (IEC) controls and powers the instruments via each of their electronics boxes, and a set of harnesses with their own Harness Radiator connects the IEC to the ISIM. Mounted on the −V1/+V3 side of the spacecraft, the Fixed ISIM Radiator (FIR)[9] and Aft Deployable ISIM Radiator (ADIR) passively reject heat from the instruments.

The JSC Chamber A thermal-vacuum test facility, the second largest thermal vacuum facility in the United States, is a 16.8m diameter x 27.4m high cylindrical vacuum vessel. It was modified extensively to accommodate the OTIS payload and to simulate a flight-like thermal environment[10]. Figure 3(a) shows the cross-sectioned CAD model of the OTIS test payload cocooned within a series of shrouds inside the JSC Chamber to provide the desired thermal environment, while Figure 3(b) displays the equivalent thermal model. The outermost wall is the ambient temperature pressure vessel; the LN_2 Shroud is the first layer inside the chamber walls, flowing liquid nitrogen at approximately 77 K during cryo-stable conditions; the innermost layer is the Helium Shroud which cycles gaseous helium at 20 K through a 12 kW capacity helium refrigerator. During the test, the gaseous helium from the refrigerator that cools the innermost shroud was distributed to 16 zones through a valve system. The helium shroud used seven zones, and the remaining nine zones were plumbed to various GSE. As all of the gaseous helium within the shroud originated from
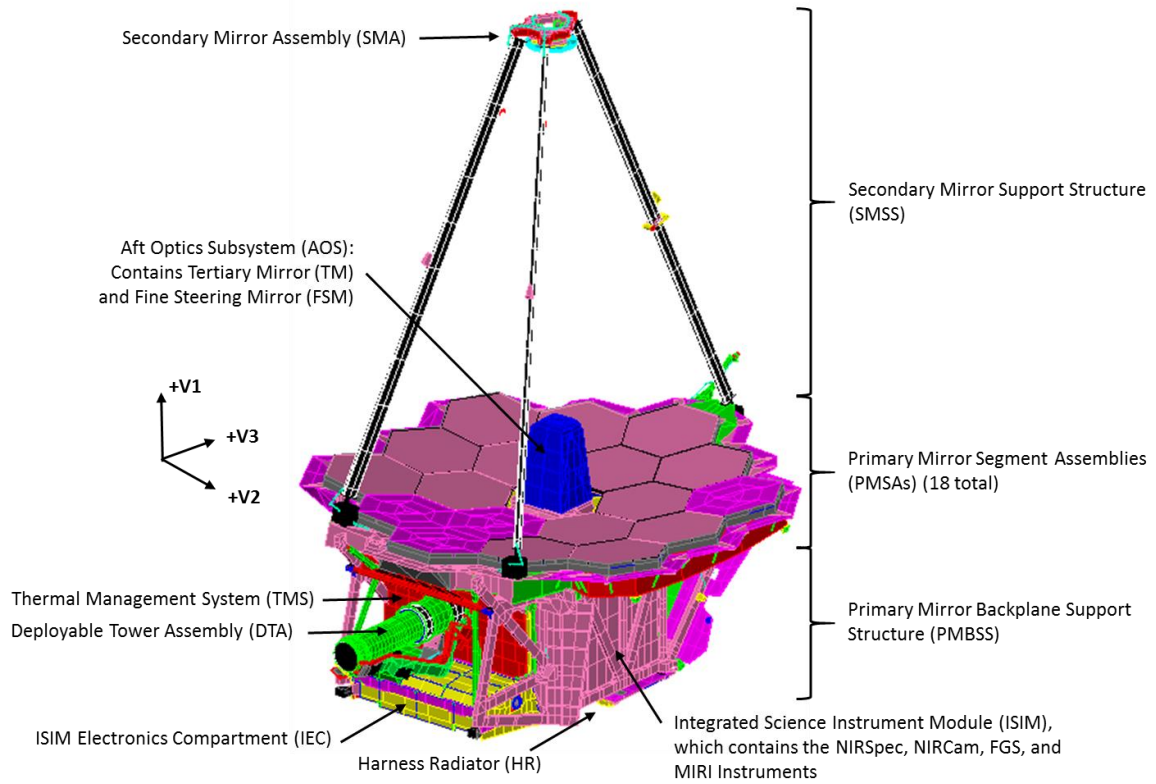
4

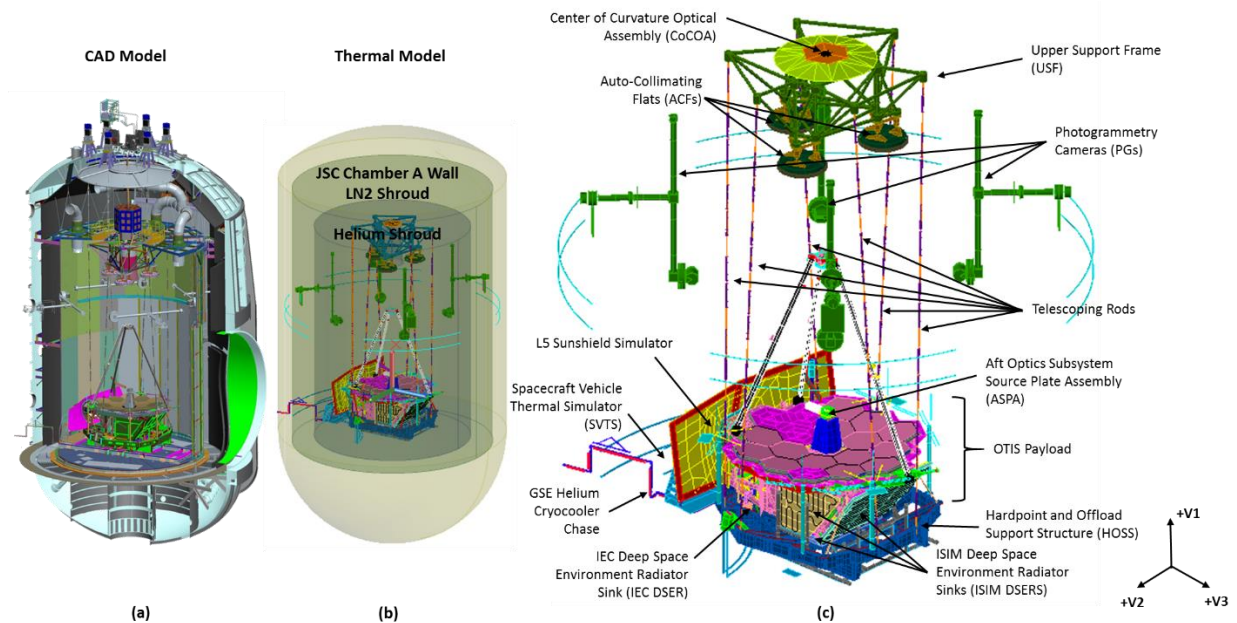**Figure 2. The OTIS CV Payload Thermal Geometry Model, Showing Major Payload Components**

Figure 3. OTIS CV Test Configuration (a) as represented in the CAD model, (b) as represented in the thermal model with chamber and shrouds, (b) denoting components in the thermal model within the helium shroud

5

a single refrigerator, the gas inlet temperature delivered to all zones was the same. Some zones additionally had line heaters to fine-tune the temperatures reaching their respective GSE.

Harris Corporation developed the complex suite of thermal GSE inside the helium shroud, as shown in Figure 3(c), to provide the correct OTIS payload thermal boundaries[11]. The Space Vehicle Thermal Simulator (SVTS) simulated the correct thermal heat loads of the JWST spacecraft and harness interfaces in the absence of the final flight spacecraft bus and sunshield. The SVTS insulation was closed out to the DTA. A truncated Layer-5 (L5) sunshield simulator attached to this "hub" region around the DTA and allowed for flight-like reflections on the payload. Mounted on frames from the helium shroud floor, a series of extremely high emissivity radiator surfaces known as the Deep Space Environment Radiators (DSERs), provided localized cold sinks for both the ISIM enclosure and IEC, and allow for separate radiative control of these components. Each DSER was a Z307-painted open aluminum honeycomb plate which measured an emissivity

Figure 4. The test configuration for the OTIS Payload inside NASA Johnson Space Center's Chamber A Cryogenic Vacuum Facility

of 0.98 at ambient conditions and 0.95 at cryogenic temperatures. The IEC DSER was controlled by a separate helium circuit to provide appropriate sink temperatures to the ambient-temperature IEC and installed electrical boxes during transitions, and also to provide for emergency safing in the event of specific unplanned failures of GSE and/or flight systems in test. Finally, the OTIS payload itself was supported on the massive stainless steel Hardpoint and Offload Support Structure (HOSS) through a series of monopod and bipod hardpoint struts, which interfaced the BSF at the −V3 and +V3 ends on either V2 side. The HOSS was helium-cooled and suspended from the ceiling of Chamber A through a series of telescoping rods, which accommodated structural shrinkage at cryogenic temperatures. Other support equipment, such as the Center of Curvature Optical Assembly (CoCOA), Auto-Collimating Flats (ACFs), and Photogrammetry Cameras (PGs) did not have a thermal function, but were employed to conduct optical testing of the OTIS payload. The Aft Optical Subsystem Source Plate Assembly (ASPA), separately developed by BATC, was mounted on the OTIS payload Aft Optics Subsystem forward bulkhead to provide sources for optical testing. The as-built configuration of the OTIS test is shown in Figure 4.
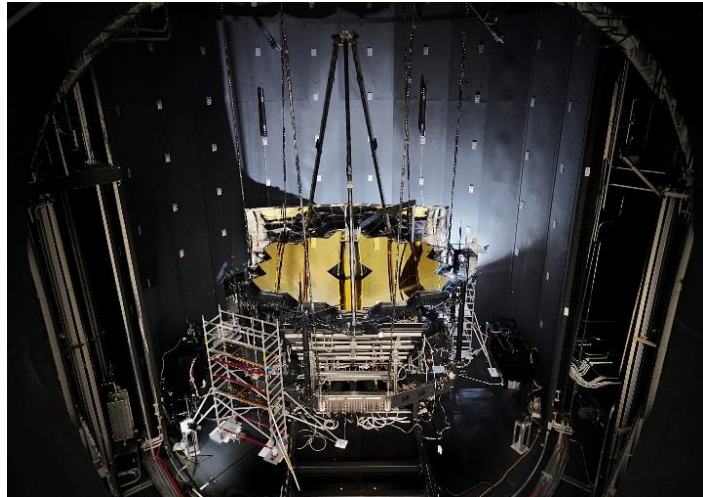
In the OTIS CV test, the primary source of heat on the OTIS payload was from the IEC, kept at 278 K to ensure the instrument electronics boxes remained within their operating temperatures. The −V3 side of the payload also saw heat from the SVTS and L5 radiating to the payload thermal management system (TMS), which isolates the cold optics and instruments. The IEC rejected most of its heat in the −V1 direction through its radiator to the IEC DSER. Any harness parasitic heat loads conducting from the IEC were further rejected via the Harness Radiator to its own DSER before they entered the cryogenic instruments. Within ISIM, the MIRI optical bench was actively cooled to 6 K via a cryo-line leading to a GSE cryocooler. The Near IR instruments and the MIRI instrument kinematic mounts were passively cooled via high-purity Aluminum 1100 heat straps to their respective radiators on the FIR and ADIR. The ISIM DSERs facing these instrument radiators provided the final sink for payload heat. In flight, the FIR and ADIR provide ample cooling for the ISIM instruments to reach their operational temperatures, but the cool-down duration, at approximately 90 days, was not acceptable for ground testing. To accelerate the temperature transition to instrument operational temperatures, additional ISIM GSE "pre-cool" heat straps were attached to the flight heat-strap radiator interfaces, allowing for added conductive heat flow out to a GSE helium line, which is especially significant at low temperatures where radiation heat transfer is less effective. These pre-cool straps were made adiabatic ("zero-Q'd" i.e., thermally non-conducting) by heaters when the payload approached and achieved thermal balance conditions by matching the temperature profile in the pre-cool straps to the temperature of the flight hardware. The hardpoint struts which supported the BSF had similar zero-Q heaters to prevent non-flight-like heat transfer across the GSE-payload interface. The primary heat paths through the OTIS test are shown in Figure 5.
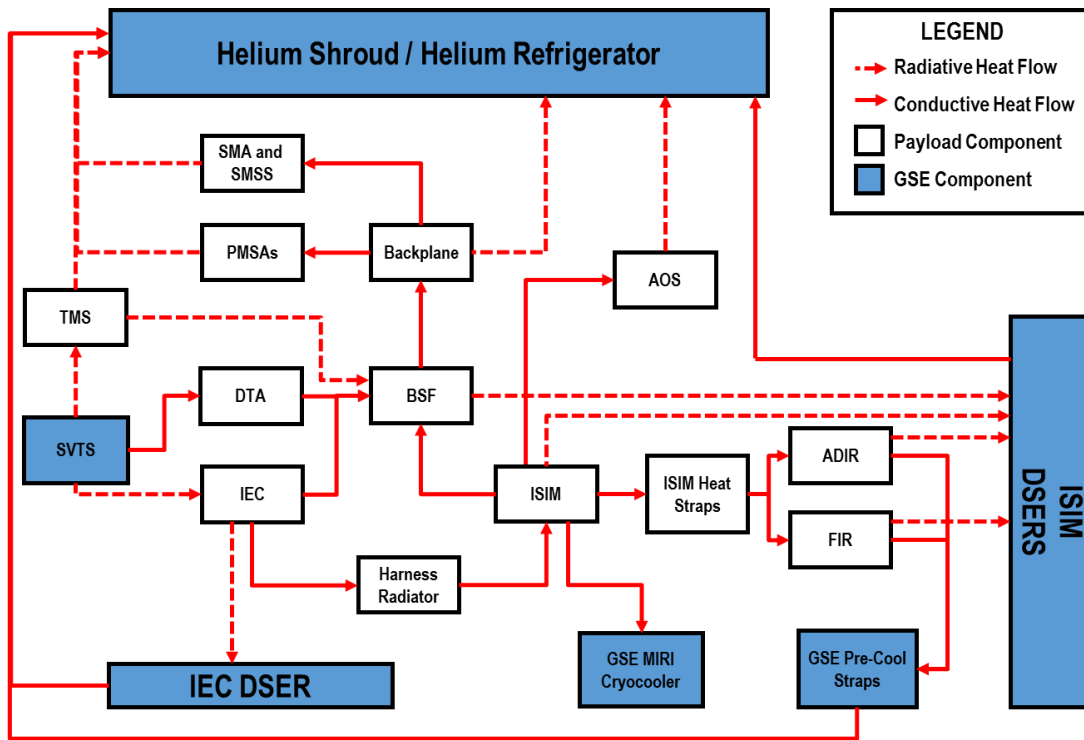
International Conference on Environmental Systems

Figure 5. Map of Primary Heat Flows within the OTIS CV Test Configuration

III. OTIS CV As-Run Temperature Profile

The OTIS CV Test was budgeted for 93 days from the pre-test chamber pumpdown to post-test chamber re-pressurization. A series of 92 thermally-related hardware L&Cs governed the cooldown, cryo-stable, and warmup phases of the test. The goal of the pre-test model was to develop an optimized method to control the test environment which transitioned the payload as quickly as possible from ambient conditions to cryogenic operating temperatures, then back to ambient, while preventing any L&C violations. While certain test phases could be optimized, others contained so many competing constraints that there was only one way to execute the thermal transition while ensuring hardware safety. As a testament to the success of the OTIS CV test model, the as-run test transient schedule nearly exactly matched the pre-test predictions.

After chamber door closure, the pressure inside the chamber dropped to the 10^{-6} torr scale, after which ambient vacuum testing of the instruments was performed. The scavenger plates inside the chamber were lowered to LN_2 temperatures to capture any molecular contamination. However, the cold sink provided by the scavenger plates in the chamber resulted in some temperature and gradient violations on the payload. Initially, it was not thought that there would be a significant ambient impact on the instrument L&Cs due to the small size of the scavengers relative to the OTIS payload. As such, this case was not part of the transient thermal simulation. During the multiple days of ambient testing, though, some components cooled enough to enter a range where molecular contamination constraints became a concern. Entering this range was not intended in the test plan until the beginning of the cooldown phase, where the temperature transition of the helium shroud environment and DSERs would allow the contamination constraints to be maintained by the natural gradient formed in the payload. Thus, at ambient, prevention of contamination of instrument optics necessitated instrument heaters to be turned on to prevent the optics from becoming colder than their surrounding environment.

Cooldown of the helium shroud began on day 8 of the OTIS CV test. The OTIS helium shroud was in-practice limited to a rate of 1.5 K/hr, following a safety standard set by the Thermal Pathfinder test. Pre-test predictions of the transition with the entire OTIS flight payload, however, showed that for the first 80 hours of cooldown in OTIS, the helium shroud rate of cooling should be decreased to 1 K/hr due to pre-test predictions of the intra-component

gradients on the PMSAs. Below 210 K on the helium shroud, it was predicted that the PMSA structural L&Cs would have peaked and begun decreasing. Indeed, this trend was observed during test, and past day 3, the helium shroud could transition to its faster cooldown rate. By day 16, the helium shroud reached 20 K, establishing the planned environment for cryo-stable testing. Due to the large thermal mass of the OTIS payload, complete cooldown of the flight hardware required an additional three weeks to reach expected stability at cryogenic temperatures (also referred to as "cryo-stable temperatures"). As seen from Figure 6, many of the more massive components, such as the primary mirrors, rapidly cooled at the outset but took up to 32 days from the start of cooldown to begin to exhibit asymptotic behavior to their steady cryogenic temperatures and achieve the 27 mK/hr stability required for optical testing. The lower thermal mass Near-IR science instruments (NIRCam, NIRSpec, and FGS) reached a planned contamination avoidance hold between days 15 and 20 of the total profile. As water contamination was emitted by the composite ISIM structure between 140 K and 170 K, the instrument optics were held above this temperature range to prevent contamination within the ISIM enclosure. Conversely, the MIRI bench, with its extreme thermal isolation, was slowest to cool during this period. Once the ISIM composite structure elements reached below 140 K and no longer emitted water, the MIRI cryocooler could be turned on to actively drive the MIRI bench temperature to 170 K. When MIRI cooled to the level of the Near IR instrument temperatures at the threshold of the water contamination band, all SI bench heaters were stepped down in 5 K increments to prevent cross-contamination from instrument-to-instrument until they were all below 140 K. The FSM, a mirror having a direct view to all of the instrument pick-off mirrors (POMs), was also subject to the same contamination requirements as the instruments themselves. The FSM was similarly held at the median temperature of the SI benches, then stepped down until water deposition was no longer a concern.
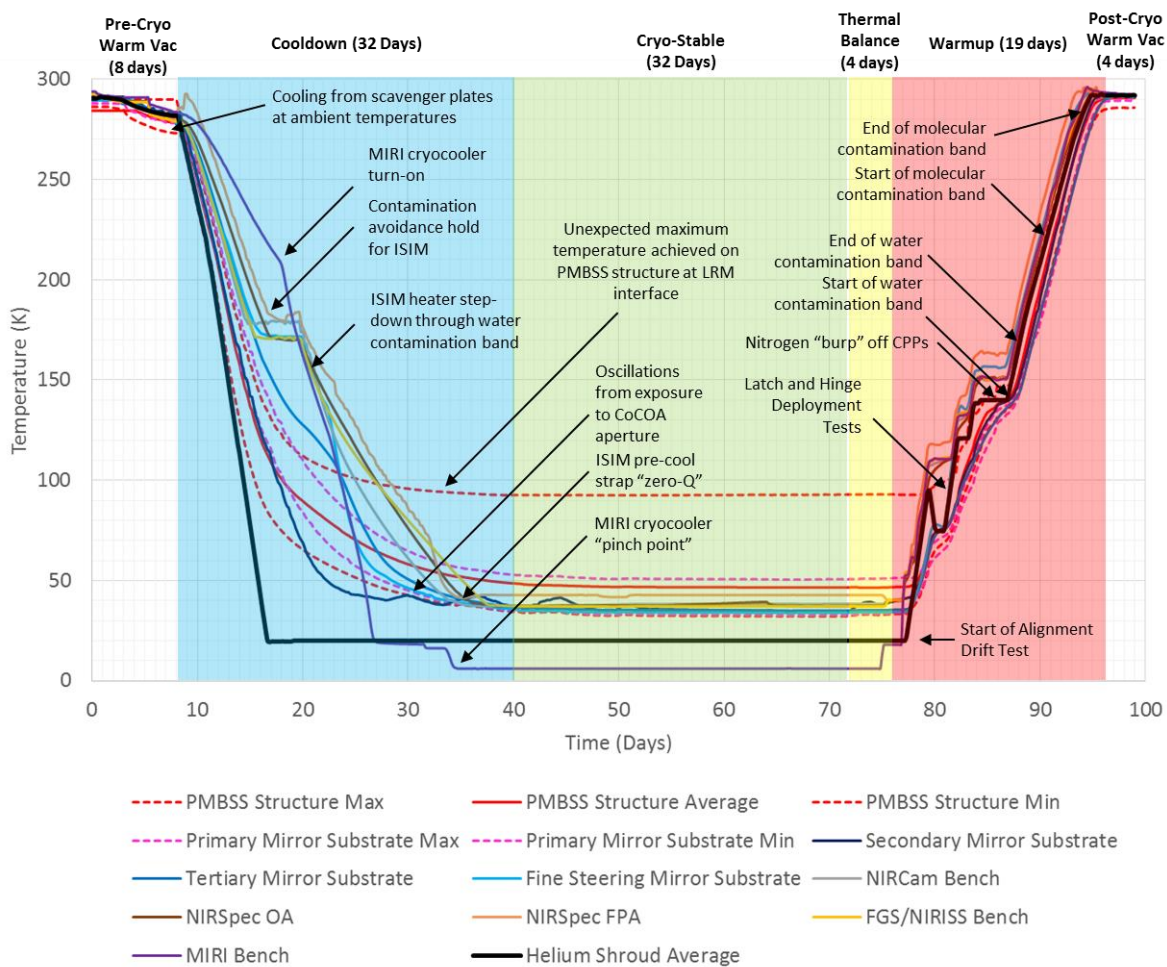

Figure 6. As-Tested Data: OTIS CV Temperature Profiles for Major Components

International Conference on Environmental Systems

Past day 20 of the OTIS test, all instrument decontamination heaters except the NIRSpec FPA were turned off to allow cooling of the instruments via their respective radiators to their cryogenic operating temperatures. At the heat strap-radiator interface, the "pre-cool" GSE heat straps provided additional conductive cooling to a separate helium line. The NIRSpec FPA heater remained on above the OA until day 32 to prevent any excess structural gradients, rapid temperature rate changes, and contamination between both assemblies, as the FPA's thermal mass was much lower than the OA. When the instruments reached their operational temperatures between 35 K and 42 K, the zero-Q heaters for each pre-cool strap interface were turned on. The MIRI cryocooler drove the MIRI bench to about 18K, after which the cryocooler transitioned from an 18 K Pulse tube cooling method to a 6 K Joule-Thomson process, as shown in the rapid drop of MIRI bench temperatures around day 34. Once operational temperatures and stability requirements were achieved on all of the primary optics at Day 40, the cooldown was considered complete and cryo-stable optical testing could begin.

Day 40 through 72 of the OTIS CV test saw an assortment of instrument and optical tests on the OTIS payload to understand the telescope's end-to-end optical performance. Thermal distortion tests were also executed at the end-of-cooldown to understand the figure drift with temperature change. Oscillations in temperature, as seen most significantly between days 28 and 50 on the SMA, were caused by the exposure of the payload to the room-temperature CoCOA aperture for interferometry measurements during optical and thermal distortion testing. From days 37 to 41, Hurricane Harvey hit the Houston, TX area, causing significant flood and wind damage[12]. Thankfully, NASA JSC did not suffer a power outage and the OTIS CV test was impacted only with a five-day optical test schedule delay. Aside from the off-nominal weather event, the cryo-stable phase was a relatively quiescent period for the thermal subsystem, and valuable information could be gained about the thermal performance. The ISIM thermal balances were performed in this phase during periods of minimal instrument activity, and permitted accurate measurements of flight heat strap conductance and radiator heat dissipation. From Day 72 through 76, the payload underwent a thermal balance of the OTE subsystem to understand the system-level cryogenic performance of the OTIS payload and provide data to selectively correlate the OTIS CV thermal model.

At Day 76 of the OTIS CV test, the cryogenic test portion was determined complete and the instruments were actively heated to 50 K in preparation for payload warmup to ambient. As the helium shroud was slowly increased in temperature, the sublimation of nitrogen off the payload and helium shroud onto cold scavenger panels between the helium and LN_2 shrouds caused a small and expected pressure rise inside the chamber. As the helium shroud temperature continued to increase at 1.5 K/hr, the shroud average peaked at 95 K before decreasing at 1.5 K/hr again to a 75 K plateau. This was in the interest of overdriving the payload for the thermal distortion alignment drift test, which required measurements of structural temperature gradients and spatial deformation at two separate, stable states: cryo-stable temperatures and 75 K average. The NIRCam, NIRSpec OA, FGS, and MIRI benches were consistently held at 10 K above the temperature of their respective DSERs, whereas the instrument pick-off mirrors were 18 K above the DSERs, and the NIRSpec FPA was 22K above them. Contamination requirements were conflicting: the DSERs could not be at risk of contaminating the ISIM enclosure by being warmer than the instruments themselves, nor could any of the instruments risk contaminating others by departing in temperature from the bulk average of the others. Therefore, through the entirety of warmup, all of the SIs and their optics, as well as the FSM which has a direct line of sight to the SI POMs, required active control to keep within 15 K of each other.

Following the end of the thermal distortion alignment drift test, day 81 saw the helium shroud resume its steady 1.5 K/hr increase towards 140 K. A short 24-hour hold at 120 K allowed for gradients within the NIRSpec bench to isothermalize. During this time, a series of latch and hinge deployment tests on the DTA, PMBSS, ADIR, and SMSS structures raised their respective deployment heaters to 300 K to ensure functionality during flight deployments of the JWST observatory. At 140 K, a longer helium shroud hold was executed as the more massive optical components caught up to the helium shroud temperature. The Cryo-Pumping Panels (CPP), cold contamination collectors between the LN_2 and helium shrouds, were raised in temperature at a controlled rate during this time to sublimate their collected residual air-leak N_2 and allow them to be pumped out via the chamber cryo-pumps. An expected rarefied "burp" of nitrogen gas was released inside the chamber, and in general the increased gas coupling between surfaces lowered payload gradients. However, this event also caused unexpected approaches towards temperature limits as greater coupling between surfaces caused increased heat transfer between the composite shell of the room-temperature IEC and its cold environment. Mitigation steps were taken to halt the CPP warm-up and allow the pumps to lower the pressure. When the pressure was at an acceptable value and the risk of hardware damage was minimized, the CPPs continued to warm until the completion of the "burp." This mitigation prevented the IEC shell temperature from

9

exceeding its limit. Afterwards, the helium shroud resumed its temperature increase, albeit at a slower rate now due to contamination requirements. Between 140 K and 170 K, water release from the composite structure could act as a contaminant for the optical surfaces, and therefore the PMs, SM and TM could not lag the helium shroud by more than 35 K to reduce any chance of deposition in this contamination "band." Above 220 K, the release of molecular contaminants further posed a risk to the optics. Hence, for the entire temperature regime from 140 K to ambient, the helium shroud rose at the rate of 0.6 K/hr to 0.8 K/hr to ensure that all optical components and instruments would be able to consistently maintain their required ΔTs with respect to the helium shroud. When the SIs finally reached above 295 K, their heater powers were cascaded down to zero to meet the helium shroud temperature. The helium shroud was slightly overdriven to bring all of the lagging optical components to above 290 K, the requirement for the end of the warmup phase. From day 96 onwards, the post-vacuum ambient functional testing phase was executed for an additional four days before declaring the end of the test.

IV. Thermal Model Performance against Test Data for Cooldown and Warmup

The comparisons for major components between pre-test temperature predictions and the measurements taken during the OTIS CV test are shown in Figure 7 for the ISIM and Figure 8 for the OTE. Dashed lines represent pre-test predictions and solid lines represent test measurements. The operational assumptions used in the pre-test predictions were not always consistent with the as-run operations. For instance, thermal related contamination control L&C's were modified in real time during the test; other significant deviations are explained below. Despite this, the overall comparison between major component temperatures during cooldown was very good except for a PMBSS structure maximum temperature anomaly discussed later in this section. The model captured both transient and steady-state cryo-stable behavior of the payload well, and was able to anticipate all major areas of concern with respect to L&Cs, allowing the OTIS team to plan well in advance the correct environmental controls to ensure hardware safety.
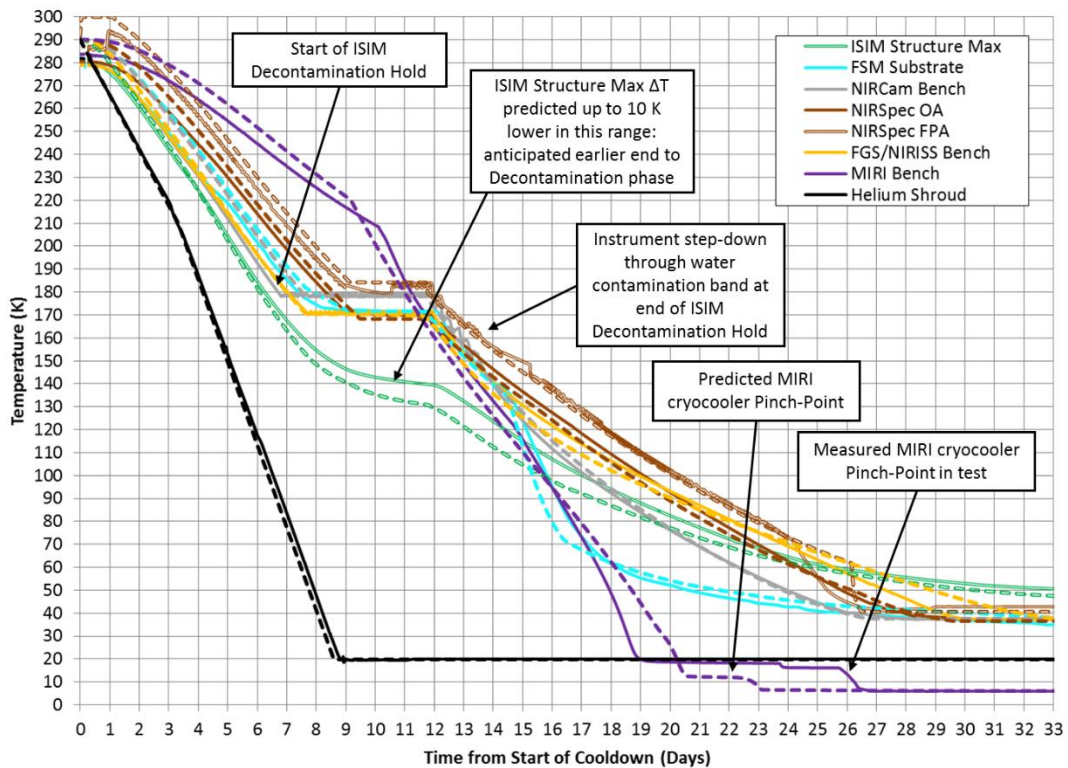

Figure 7. Temperature Comparison for ISIM Components between Model Predictions (Dashed) and Test Measurements (Solid) during Cooldown

The prescribed helium shroud cooldown profile, determined by pre-test predictions, was matched extremely closely by the JSC facilities team, including the helium shroud rate transition past day 3 of cooldown. The actively-heated instruments all followed their prescribed cooldown profiles closely, indicating that the thermal mass and heat paths out of each of these instruments was captured correctly by the thermal model. The near-IR instruments were all held at above 170 K starting on day 7 for the ISIM decontamination hold, then stepped down on day 12 through 14 after MIRI was actively cooled to be in-family with the near-IR instrument temperatures. The cooldown of MIRI below 140K is governed specifically by the operation of the cryocooler. MIRI operated in its Pulse-Tube cryocooling mode with cold helium circulation through the cryocooler line and MIRI bench, bypassing the Joule-Thomson cryocooler, until the MIRI optical module reached 18K. Below 18K, a "pinch-point" occurred where circulation was disabled to the bench and the Joule-Thomson cryocooler was turned on, driving the bench to 6K. As the model predicted pinch-point occurring at day 22, whereas in test it actually occurred on day 26, there is a perceived discrepancy in time between model and test. However, this is not an inaccuracy in the model predictions: since the MIRI cryocooler is an actively-controlled thermal system, the transition of modes at pinch-point is purely determined by the parasitics on the cryocooler line and the judgment of the cryocooler team, rather than a predetermined time. The FSM, which tracks the instrument cooldown, was actively controlled via a baseplate heater to achieve all contamination-prescribed ΔTs with respect to the science instruments. However, the heater was not directly mounted to the FSM mirror substrate that it sought to control and the weak thermal coupling between the FSM baseplate and the substrate made it difficult to center the FSM substrate temperature to the median of all of the instrument temperatures. Active control of the FSM and instrument heaters were not needed when all of these components were below 140 K, and indeed their cooldown profiles were better matched by the thermal model after day 14.
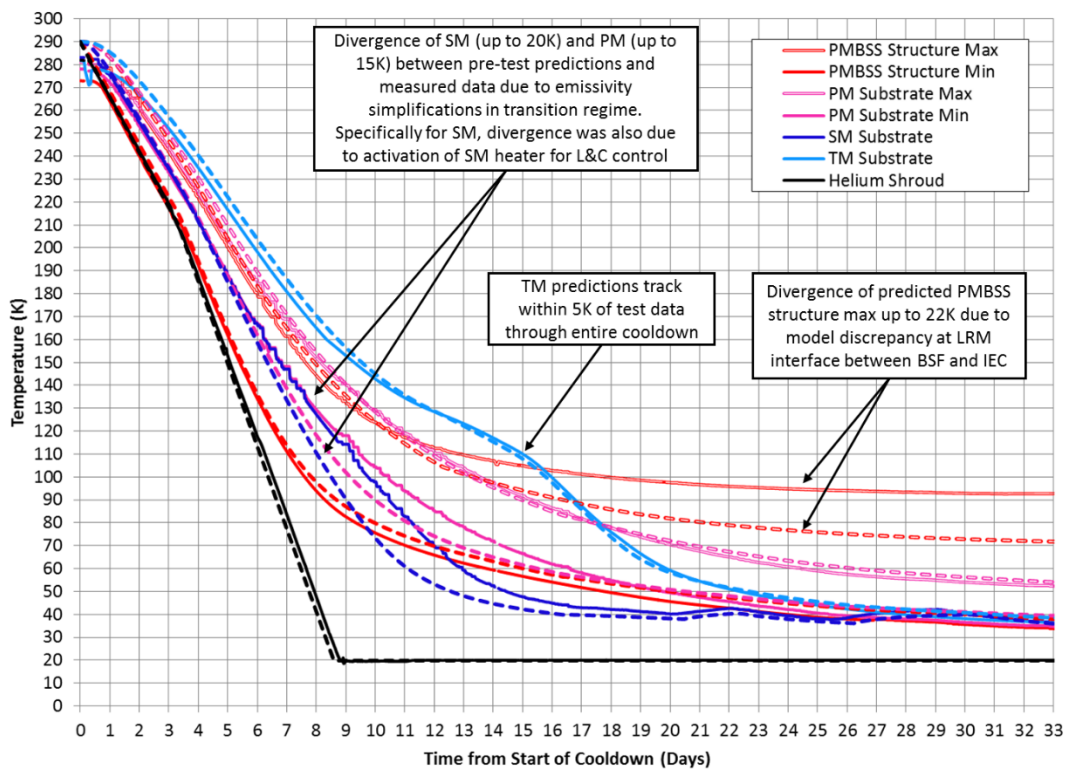

Figure 8. Temperature Comparison for OTE Components between Model Predictions (Dashed) and Test Measurements (Solid) during Cooldown

For the OTE optics, the primary mirror predictions followed very closely from ambient temperatures through 170 K. However, below 170 K, especially on the colder PMs, the predictions began diverging significantly from test measurements, up to 15 K difference at 90 K average temperature. Towards the cryo-stable phase, the predictions and measurements converged again. An investigation into the difference between model predictions and test in the temperature regime between 60 K and 170 K pinned the model error to temperature-dependent emissivity assumptions.

11

This was recognized and studied earlier in the model development and in the interest of runtime for the OTIS CV thermal model, only two emissivity sets were deemed sufficient: a room-temperature emissivity set when the PMBSS average was above 90 K, and a cryo-emissivity set below 90 K. Separate radiation conductors were calculated for each set, and the model transitioned between these sets of conductors once it determined that the PMBSS average fell below 90 K on cooldown. However, this simplification failed to account for the complex interactions between those surfaces with temperature-dependent emissivities, especially in this temperature transition regime. It also did not consider that, at any given time window in the transition, the different cooldown rates of each surface resulted in higher temperatures and emissivities for more thermally massive components, and lower temperatures and emissivities for lighter hardware such as soft structure. Therefore, the assumption of room-temperature emissivities on all surfaces was entirely valid only when all components were at room temperature, and the same statement for cryogenic emissivities could only be made when all surfaces are at cryogenic steady-state. When the model predicted transient temperatures on the payload before the emissivity set transition, it overestimated the emissivity on all components, but especially those components which were less massive and reach colder temperatures quicker. Conversely, after the emissivity set transition, the model underestimated the emissivity on all components, but especially those components which were more massive and still warm even after the emissivity switch at 90 K PMBSS average. Hence, this explained the trend observed on the PM substrate minimum temperature between 60 K and 170 K: before the emissivity transition, the model overestimated the PM emissivity and predicted colder than test measurements; after the emissivity transition, the model underestimated PM emissivity, resulting in a slower cooling rate than measured and allowing for model and test results to converge towards cryogenic steady-state. A similar trend was seen on the secondary mirror substrate, but this divergence between model and test was both due to the emissivity transition as well as another factor: the use of the secondary mirror heater. Initially in the OTIS CV test, the SM had a stringent constraint for allowable temperature differences between its constituent components, each with different thermal masses. The emissivity simplifications reduced the model's accuracy to predict cooldown rates for each individual SM component, and did not detect that there would be an exceedance of SM component-to-component L&Cs in this transition regime. Since in the test it was observed that ΔTs between SM components were much larger than predicted, it became necessary to power on the SM heater to drive down intra-SMA gradients. While later it was found that the incorrect L&C was being applied to the SM in test and as such it did not require active heater control, the prediction inaccuracies due to emissivity were still a significant contributor to the large divide between model and test temperatures, in addition to the positive control exerted by the SM heater.

The correct prediction of ΔT between maximum and minimum temperatures on the PMBSS structure was critical for the OTIS CV test since there was a very stringent temperature-dependent allowable ΔT requirement set forth from earlier subsystem-level testing, and any exceedances of this allowable limit place the composite structure at risk of hardware damage. The pre-test predictions for the cold end of the PMBSS structure generally matched well with test measurements. Certain less-massive components, such as those composite beams and structural extensions with a direct view to the cold helium shroud, reflected the same error between model and test as the PMs due to the emissivity set simplification, but were less severe in temperature difference than the PMs. However, on the PMBSS structure maximum temperatures, the model predictions started diverging versus test at about 120 K, and reached a measured quasi-steady value at cryo about 22K higher than model predictions. This egregious difference between model and test results was extremely surprising to the OTIS team at first, given that the model generally predicted within ±3K for all other major components. Subsequent investigation found that this temperature difference was restricted to the launch release mechanism (LRM) interface between the room-temperature IEC and the cold BSF, at a titanium mechanical flexure. The bulk of the other sensors spread through the PMBSS structure showed close matches between model and test, and assessments by the structural team proved that this localized hot spot at the LRM interface had a negligible impact on the structural integrity of OTIS. Additional investigations found that about 7-8 K of the discrepancy between model and test could be attributed to an error in modeled conductance through this interface. Due to this area being sandwiched between the hot electronics boxes and cold BSF structure, a 160K gradient existed in this region, and small changes in model conductance values resulted in large changes in predicted temperature values. However, an additional 11 K of discrepancy is still unaccounted for even with currently-implemented thermal model fixes; the investigation is still ongoing as to determining the root cause of conflict between model and test at this interface.

The overall accuracy of the model at thermal balance in cryogenic temperatures versus test measurements is shown in Figure 9. In total there were over 1000 payload thermal sensors on this very large test article. This histogram shows the ΔT of model predictions minus test data for all hard structure sensor locations. The steady-state comparison of

12

model to test showed extremely good correlation: over 90% of all test sensor measurements were matched within ±4 K by model-predicted values at corresponding sensor locations. This gave strong confidence that the OTIS CV thermal model captured accurately the payload behavior in the cryo-stable test environment, and further provided assurance that the flight model would be an accurate predictor of temperatures on-orbit, since the OTIS payload model was directly sourced from the flight model. The bulk average of all of the predicted temperatures to their corresponding measured sensors was extremely close: within 0.1 K. Even so, it was noticed that sensors around the SVTS, IEC, and DTA region predicted slightly warmer in the model than in test. This effect was eventually attributed to the blanket performance on the IEC. The OTIS payload model assumed a conservative ε* value of 0.03 for IEC MLI through-thickness effective emissivity, carried over from the flight observatory model. This allowed more heat to escape from the warmest payload components inside the chamber (the room-temperature instrument electronics boxes) and raised the background sink temperature of the entire modeled test environment. However, in test, the IEC released less heat than expected to the environment due to two factors: the conductance from the IEC to the supporting GSE struts was correlated from test data to be greater than predicted, reducing the amount of radiated heat; and the assumed ε* value of 0.03 was too large given the BOL properties of the blankets. This contributed to a lower background sink temperature. Hence, the sensor measurements over the payload were consistently lower in temperature than model predictions.
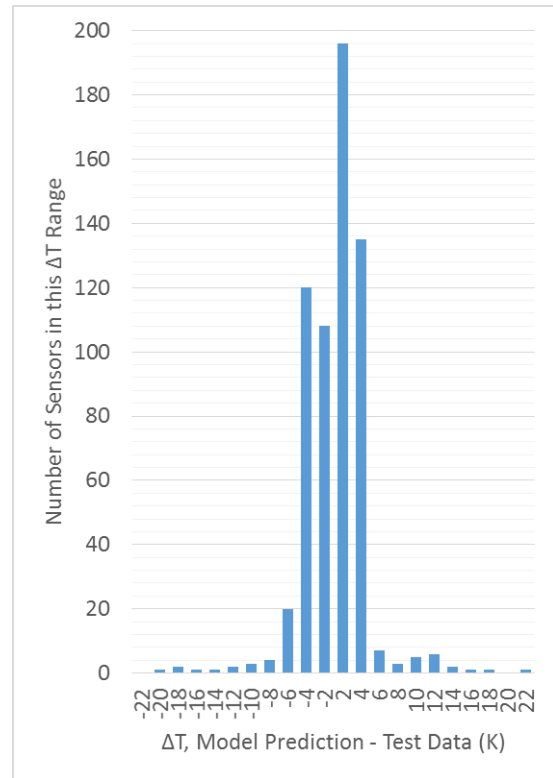

Figure 9. Comparison of Model Predictions and Test Data at Thermal Balance

On warmup, the response of the payload was less well-matched temporally between the model and test results, as shown in Figure 10 for the ISIM and Figure 11 for the OTE. In the first phase of warmup, the thermal distortion alignment drift test was executed as the PMBSS and SMSS were driven as quickly as possible to sub-100 mK/hr stability at a 75 K average, comprising a "State 2" stable condition for photogrammetry measurements of the OTIS payload structural geometry. The model predicted that this overdrive maneuver on the structure would necessitate the helium shroud increasing at 1.5 K/hr to a 105 K average, then decreasing to 75 K, after which it would hold constant at 75 K until both the PMBSS and SMSS were below their temperature rate requirements for "State 2" data acquisition. In actuality, the payload structure responded much more quickly than expected. From pre-test analysis, it was understood that a "trigger point" for reversing the helium shroud rate occurred when the PMBSS structure average reached 71 K, corresponding to the time when the shroud peaked at 105 K. In test, the PMBSS reached this average temperature when the helium shroud was only at 95 K; this required immediate response from the thermal team to turn the helium shroud rate to -1.5 K/hr and stem the rise of the PMBSS and SMSS temperature, as well as to prevent a much longer recovery time to stability. Furthermore, during the hold at 75K, the payload reached its thermal stability much faster than expected. The entire alignment drift phase completed one full day earlier than planned: it was found that the faster overall payload response and inability of the model to predict this schedule accurately was again due to the cryogenic-to-room temperature emissivity set transition. As the payload rose above cryo-stable temperatures, the assumption of cryogenic emissivities was no longer completely valid, and therefore the model underestimated the amount of heat transfer actually occurring on the payload. As such, the model response was slower and more temporally conservative than what was observed during the test.

Beyond the end of the thermal distortion phase on day 5, the test results matched model predictions fairly closely. The duration of the helium shroud rise to 140 K and subsequent payload response was similar to expectations from pre-test analysis, save some differences in localized PMBSS temperature rise due to deployment heater testing. The length of the 140 K helium shroud hold, however, differed due to the risk mitigation steps taken as a result of increased coupling of payload components during the large N2 "burp", as discussed in the previous section. The model did not

13

simulate the complexity of free-molecular then convective heat transfer during this event and therefore did not capture the correct temperature distribution across the payload before the start of the next phase. Into the water contamination emission band between 140 K and 170 K and during the molecular contamination emission band above 220 K, the model consistently predicted a slower warmup rate than was executed during the test. The helium shroud warmup rate was driven by the contamination constraint to maintain all of the OTE optics within 35 K of the average helium shroud temperature during this phase. The original pre-test thermal analysis stacked worst-case conditions to predict warmup through these contamination bands with ample schedule conservatism, excluding the benefits of gas heat transfer during the nitrogen burp to bring the mirrors closer to the helium shroud temperature, as well as allowing for interim holds to keep all of the instruments at least 10 K above their adjacent DSERS temperatures in accordance with contamination limits. Given these constraints, it was determined through thermal model predictions that the helium shroud rate would need to decrease to as low as 0.5 K/hr average to maintain the coldest PM no lower than 35 K below the helium shroud and "ride the yellow line" with respect to contamination limits. When it was observed in test that all of the OTE optics and instruments could maintain a faster rate with respect to the helium shroud without violating any constraints, and it was deemed acceptable by the contamination control team that the instruments only lead the ISIM DSERS by 6.5 K in the interest of schedule, the helium shroud was sustained at 0.6-0.8 K/hr through the end of warmup. Therefore, the completion of warmup actually occurred almost two days earlier than pre-test predictions.
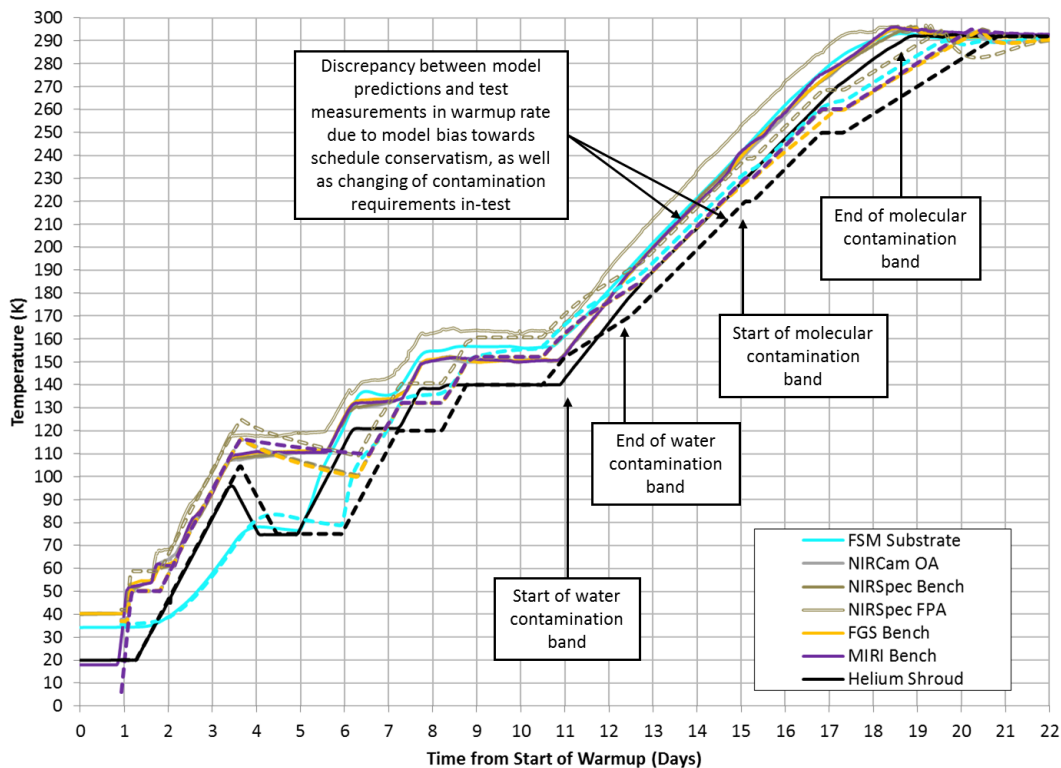

Figure 10. Temperature Comparison for ISIM Components between Model Predictions (Dashed) and Test Measurements (Solid) during Warmup

Two OTIS model configuration-specific issues most affected the predictive capability of the thermal model and increased the complexity and difficulty of executing the test: (1) the FSM and TM imposed heater powers, and (2) the variations between PMSA's modeling detail. Regarding the first issue, the FSM and TM assemblies only contained one sensor each, a decision made early in the JWST project due to the scarcity of telemetry channels. However, there were also extremely stringent L&Cs imposed on both components, both for structural and contamination reasons, that arrived late in manufacture and which required knowledge of temperatures on various subcomponents of each mirror assembly. As there was no sensor on either mirror substrate, a real-time, reduced thermal model[13] was created for both the FSM and TM which, when operated in conjunction with the OTIS CV test data acquisition system and temperature telemetry from sensors surrounding each assembly, provided an estimate to the mirror substrate temperatures with a

14

temperature-varying uncertainty band every two minutes based on the past couple of timesteps of data acquisition. Temperature deltas both between mirror assembly components and from mirror substrates to the helium shroud could be calculated with these inferred "virtual sensor" temperatures.
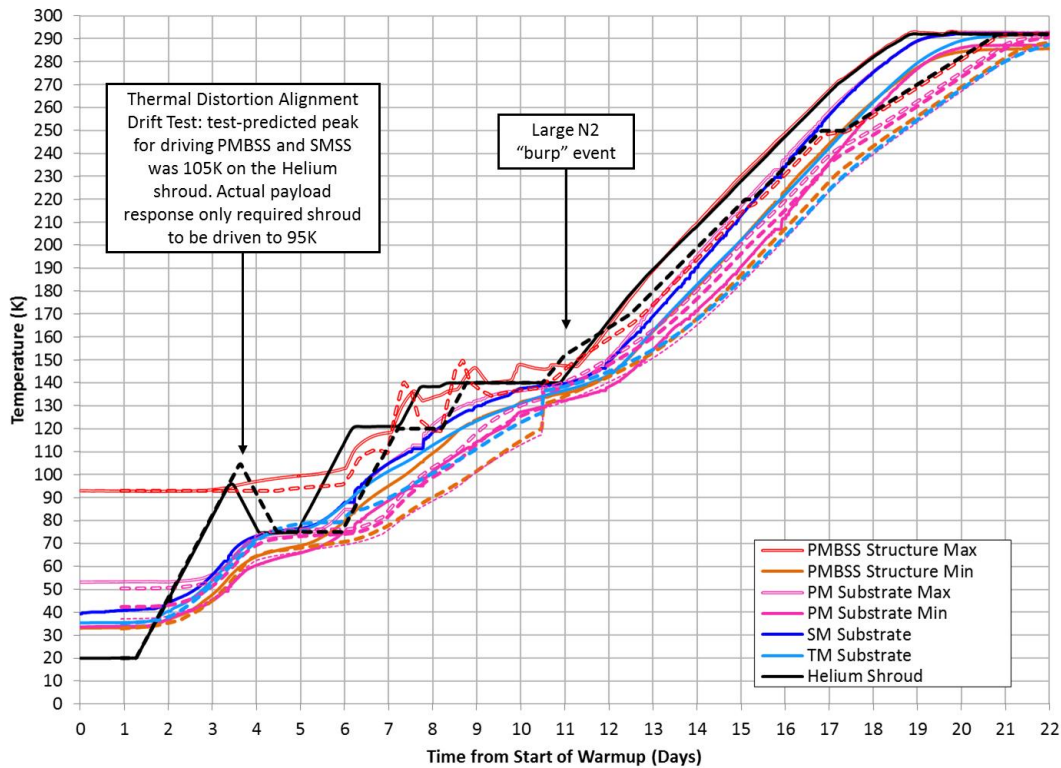

Figure 11. Temperature Comparison for OTE Components between Model Predictions (Dashed) and Test Measurements (Solid) during Warmup

Both the FSM and TM substrates had the added disadvantage of indirect control with thermal hardware: since there was a project-level requirement to forbid mounting of heaters directly to the mirror substrates, the FSM heater was mounted to its mirror assembly baseplate, whereas the TM heater was mounted to its assembly sub-bench. Both heaters, originally installed for transient test control, could only indirectly affect substrate temperatures through weak linear and radiative coupling, rather than direct conduction. This contributed to a slow substrate response time to changes in heater power in both assemblies, and exacerbated the temperature gradients between components when the heater was turned on. While the "virtual sensors" provided feedback for heater operations, there was also a reliance on model pre-test predictions to determine the heater power per test phase of the test to ensure that the FSM and TM complied with all L&Cs. The FSM heater was operated for both cooldown and warmup, while the TM heater was only used with a low power input during warmup to prevent it from becoming the schedule-driving coldest mirror.

The OTIS CV test, both in cooldown and warmup, saw the FSM requiring significantly more heater power at the FSM baseplate than model pre-test predictions had prescribed. Especially during test phase transitions, the model predictions for heater power required (such as when the FSM tries to follow the ISIM bench values during the decontamination hold in cooldown) were significantly under-predicted versus what was needed by the hardware. While some of the discrepancy can be attributed to the faster pace of warmup in the OTIS CV test, post-test investigations showed the bulk of the problem with the pre-test heater power predictions to be twofold: first, the model only predicted the heat that was required to dissipate on the FSM baseplate, where the heater was mounted, but inadvertently neglected the significant I^2R losses due to the low thermal conductivity, high electrical resistance section of the flight harness. The operations team also applied the prescribed heat to the entire circuit, which encompassed the line lengths from the power source outside of the chamber to the payload; this resulted in less-than-prescribed power at the FSM baseplate. This increased the required heater power at the source to achieve the desired heater power

15

at the FSM baseplate, since considerable heat was dissipated in the wires. In an aside, the flight model includes all of the flight harnessing losses. Second, the model assumed that there could be instantaneous jumps to heater power whenever transitions occurred, but neglected the limitations of the hardware transition rates. These two differences between the analysis and the as-run contributed to the inaccuracy to predict prescribed FSM heater power, and resulted in many ad-hoc and immediate changes to the FSM heater power during the test to ensure that it remained within its L&Cs.

The second issue from model configuration related to the difference in PMSA models used in test. There were two PMSA models developed for the OTIS program. Firstly, a detailed model had all of the PMSA component geometries in three dimensions with 32 nodes per mirror segment. This model was specifically developed to address the modeling accuracy needed in a faster and more stressful transient environment in test than on orbit. The other model is a more reduced PMSA model, which only had one node per mirror segment and simplified two-dimensional representations for all of the PMSA components. The simpler representations were the historical models that sought to reduce run times and focus on cold, steady state conditions. Originally, the motivation for implementation of the simplified PMSA model stemmed from its usage in flight model predictions, in which commissioning is a longer duration than test could afford, and so flight steady-state runs are sufficient to capture PMSA behavior with accuracy and are much faster to run. In the OTIS CV thermal model, which was made more detailed, four segments were modeled with the detailed PMSA, whereas the rest use the simplified PMSA. It was intended during OTIS test model development that the detailed model would be required for all 18 segments to capture PMSA behavior during transitions. However, replacing all segments with detailed PMSA models made model size prohibitive and severely slowed down runtime due to the ballooning number of radiation conductors from the detailed mirror segments to their surrounding test environment. It was therefore decided that only the four segments with the most extreme responses to their surrounding environments (i.e. largest component-to-component ΔTs) would be replaced with the detailed models as a high-fidelity witness for PMSA intra-component gradients, whereas the rest would remain simplified. At cryo steady-state, both the simplified and detailed models produced comparable results, and replacing just four PMSAs with detailed models was a reasonable compromise to make. In transition during cooldown and warmup, though, this became a much more difficult modeling decision to justify: the difference in PMSA intra-component gradients was extremely large when predicted by the detailed or simplified models, especially at the beginning of cooldown, when allowable ΔTs were most restrictive. The detailed PMSA predictions, while not capturing the magnitude of the largest ΔTs between PMSA components, at least managed to capture the shape of the ΔT curve correctly to what was observed in test. The simplified model, however, was completely incorrect in both the shape and magnitude of the curves, and proved useless as a predictive tool for monitoring compliance to the PMSA L&Cs in a highly transient environment. De-ratings were built into the test design in advance and the magnitude of the PMSA ΔTs never exceeded 60% of constraint plus margin, and hence there was no hardware safety issue posed by the inaccuracy of the simplified models. Had the hardware response been larger than observed, this shortcoming in the thermal model may have caused significant schedule delays in slowing down the helium shroud transition rate to prevent hardware damage.

V. Conclusion

A large thermal modeling effort was performed preceding the JWST OTIS CV test at NASA JSC to predict schedule and ensure hardware safety. Despite some discrepancies due to modeling assumptions and simplifications in the interest of runtime and test schedule, the OTIS CV thermal model in total performed exceedingly well at understanding the payload behavior during transitions from ambient to cryogenic temperatures, as well as in steady-state predictions at cryogenic thermal balance, especially appreciating the scale of the hardware and the passive deep cryogenic cooling design. Modeling the test sequence in exquisite detail for both cooldown and warmup gave the OTIS test team insight to which of the 92 thermal L&Cs would be schedule drivers in each phase of test, as well as identified the correct "knobs to turn" to mitigate any exceedance of these L&Cs. The OTIS thermal team spent enormous effort ensuring that the payload was safe both structurally and contamination-wise before the test, and the thermal model provided a valuable guideline for what to focus on and how best to avoid any problems. It is due to this extensive and exhaustive modeling campaign that the OTIS CV test was executed smoothly and successfully. As there is no observatory-level testing planned for JWST and the OTIS CV test represents the final system-level cryogenic test of the optics and instruments, the excellent match of the OTIS CV thermal model with test results also provides confidence to the flight team that the thermal models are accurately predicting the temperatures that will be seen in flight.

The lessons gleaned from this effort may prove valuable to future cryogenic missions in the interest of creating better predictive tools for hardware performance during test. Some suggestions for improving future system-level accuracy of test cryogenic thermal models are as follows. These will also be documented in NASA Goddard Space Flight Center's Applied Engineering and Technology Directorate Wiki Lessons Learned database.

- For transient cooldown and warmup predictions, especially in the transition region between 60 K and 170 K, use of more temperature-dependent emissivity sets is critical to accurately capture radiative heat transfer behavior of hardware, especially with respect to L&Cs. If dynamic calculations of temperature-dependent emissivity per analysis timestep is not an option due to large model size and prohibitive runtimes, multiple emissivity sets especially through this transition regime are a basic necessity to ensure that absolute temperature predictions on radiation-dominant components are accurate.
- Blanket performance can be a large contributor to the overall steady-state temperatures. If the observed temperatures differ from test values, it may be due to overly conservative assumptions about blanket performance.
- Transition to cryogenic temperatures and back is inherently stressful for hardware. For large scale cryogenic missions like JWST, simulation of accurate radiation heat exchange and temperature gradient-induced stresses due to the coefficient of thermal expansion (CTE) of the constituent materials may demand more detailed thermal geometric modeling. While 2D-surface simplifications of critical assemblies may be sufficient for steady-state flight predictions, it does not capture transient behavior well, especially when tracking compliance with structural limits between mirror components in a schedule-limited test. When relying on a thermal model to confirm adherence to L&Cs, it is desirable to retain detailed model geometries although they result in much longer model runtimes and hence model turn-around times, which then needs to be accommodated in the analysis schedule. Future large scale cryogenic missions should develop a modeling and analysis plan that trades the analysis speed and geometric fidelity against the program phase and accuracy goals.
- Due to modeling best-practices targeted towards creating a conservative payload model, and focused on a test start time tied to payload direct cooling but with an extended hold time near ambient in a 20K space, the transition times determined in analysis between ambient and cryogenic temperatures may tend to be longer than actually observed in test. Therefore, a good assumption to make is that overall temperature transition duration will be shorter than the model predictions.
- For areas where the model predictions did not match with test results, such as the LRM interface between the BSF and the IEC as discussed earlier, a full assessment needs to be made to determine if the observed temperatures or phenomena have a significant effect on flight performance. For this region specifically, the location of these LRM interface sensors was bound at their test-measured thermal balance temperatures in the flight model and analyzed in steady-state to understand the impact on flight metrics. It was found that this level of static, localized gradient does cause a slight degradation to thermal margins, but does not meaningfully contribute to the amount of stray light on the optics nor the performance of the instruments.
- For interfaces with large thermal gradients or temporal thermal change, a greater number of test sensors is crucial to understanding the heat flows and physical phenomena that occur at each interface in case the trends observed do not match what was expected from pre-test predictions. As discussed in the paper, much of the difficulty with diagnosing the anomaly at the BSF interface to the IEC or understanding of performance against L&Cs on the FSM and TM substrates was due to an inadequate number of test and flight sensors at those interfaces. Safety and anomaly assessment are the main reasons cryogenic systems need far more diagnostic sensors than ambient spacecraft and it needs to be recognized that this needs to be a planned expense. Furthermore, the mirror heaters being placed on separate components removed from the FSM and TM substrate made for extremely difficult control of the mirror substrate temperatures. Future missions should always make considerations for placing heaters on directly on the components they attempt to control, especially if that component has stringent structural and/or contamination requirements. This will increase hardware safety, reduce test time that can be paced by analytical uncertainty, reduce reliance and effort from system level models, and avoid undue effort post-test to troubleshoot anomalies and understand behavior.

Acknowledgments

17

References

[1]Feinberg, L., Voyton, M., Lander, J., Keski-Kuha, R., and Matthews, G. "James Webb Space Telescope Optical Telescope Element/Integrated Science Instrument Module (OTIS) Status." *Proceedings of the SPIE.* Volume 9904, id. 990407. 2016.

[2]Kimble, R., Apollo, P., Feinberg, L., Glazer, S., Hanley, J., Keski-Kuha, R., Kirk, J., Knight, S., Lambros, S., Lander, J., McGuffey, D., Mehalick, K., Ohl, R., Ousley, W., Reis, C., Reynolds, P., Begoña Vila, M.; Voyton, M., Waldman, M., Whitman, T. "Cryo-Vacuum Testing of JWST's Integrated Telescope & Scientific Instrument Suite." *American Astronomical Society.* AAS Meeting 229, id. 238.14. 2016.

[3]Park, S., Brinckerhoff, P., Franck, R., Schweickart, R., Thomson, S., Burt, W., and Ousley, W. "Successful Completion of the JWST OGSE2 Cryogenic Test at JSC Chamber-A while Managing Numerous Challenges." *46th International Conference on Environmental Systems.* Vienna, Austria, July 13-17, 2016.

[4]Ousley, W., Burt, W., and Davis, A. "James Webb Space Telescope Cryogenic Thermal Pathfinder Test" *44th International Conference on Environmental Systems.* Tucson, AZ, July 13-17, 2014.

[5]Davis, A., Ousley, W., Burt, W., and Cottingham, C. "James Webb Space Telescope Thermal Pathfinder Test Development." *46th International Conference on Environmental Systems.* Vienna, Austria, July 13-17, 2016.

[6]Davis, A., Ousley, W., and Burt, W. "James Webb Space Telescope Thermal Pathfinder Test Results." *47th International Conference on Environmental Systems.* Charleston, SC, July 17-20, 2017.

[7]Glazer, S., and Comber, B. "James Webb Space Telescope Integrated Science Instrument Module Thermal Vacuum/Thermal Balance Test Campaign at NASA's Goddard Space Flight Center." *46th International Conference on Environmental Systems.* Vienna, Austria, July 13-17, 2016.

[8]Yang, K., Glazer, S., Ousley, W., and Burt, W. "Thermal Considerations for Reducing the Cooldown and Warmup Duration of the James Webb Space Telescope OTIS Cryo-Vacuum Test." *47th International Conference on Environmental Systems.* Charleston, SC, July 17-20, 2017.

[9]Franck, R., Gurule, A., Brown, D., Brinckerhoff, P., McCallan, T., and Renbarger, M. "High Performance Cryogenic Radiators for James Webb Space Telescope." *46th International Conference on Environmental Systems.* Vienna, Austria, July 13-17, 2016.

[10]Homan, J. Cerimele, M., and Montz, M. "Creating the Deep Space Environment for Testing the James Webb Space Telescope at NASA Johnson Space Center's Chamber A." *43rd International Conference on Environmental Systems.* Vail, CO, July 14-18, 2013.

[11]Havey, K., Cooke, D., Huguet, J., and Day, R. "Thermal Management of JWST Cryo Test Support Equipment." *48th International Conference on Environmental Systems.* Albuquerque, NM, July 8-12, 2018 (submitted for publication).

[12]Glazer, S., Yang, K., Comber, B., Ousley, W., and Cleveland, P. "Off-Nominal Planning for the Cryogenic Thermal Vacuum/Thermal Balance Test of the James Webb Space Telescope Optical Telescope Element/Integrated Science Instrument Module at the Johnson Space Center." *48th International Conference on Environmental Systems.* Albuquerque, NM, July 8-12, 2018 (submitted for publication).

[13]Franck, R., Schweickart, R., and Comber, B. "The Use of Real Time Models to Produce Virtual Sensor Telemetry During the JWST OTIS Test." *48th International Conference on Environmental Systems.* Albuquerque, NM, July 8-12, 2018 (submitted for publication).